Contrib Mineral Petrol (1996) 126: 67–80

I.M. Villa · B. Grobéty · S.P. Kelley
R. Trigila · R. Wieler

Assessing Ar transport paths and mechanisms in the McClure Mountains hornblende

Received: 12 October 1995 / Accepted: 11 July 1996

Abstract We have investigated the mechanisms and pathways by which Ar diffuses through the McClure Mountains hornblende (ferroan pargasite), selected as a good example of material normally dated during Ar-Ar studies. A coarse-grained hornblende separated from the same hand specimen as the MMhb-1 age standard was subjected to a hydrothermal cold-seal bomb experiment and characterized by TEM. Heated and unheated crystals were subjected to four different $^{39}Ar/^{40}Ar$ dating extraction techniques: conventional stepwise heating, infra-red laser spot, ultra-violet laser depth profiling, and closed-system stepwise etching. The stepwise heating age spectrum reproduces the features often interpreted as resulting from a concentric diffusive zonation, but the other three techniques yield results that are not compatible with such a simple picture. The IR laser data indicate that the dependence of laboratory Ar loss on grain size, predicted by Fickian diffusion, is at best poor and instead is related mainly to mineralogical variations. The depth profiles show the importance of planar zones (spaced between <1 and >150 mm from TEM evidence) in providing fast pathways for inward diffusion of atmospheric Ar from the capsule, but showed no evidence of diffusive profiles in the bulk of the hornblende lattice. The data from closed system stepwise etching underscore the role of zones rich in planar defects both for Ar loss and for nucleation of etching. The age spectra obtained by stepwise heating suffer from the differential breakdown of impurity phases, whose presence can be diagnosed with several isotope correlation plots; particularly revealing are Cl-Ca-K trends. In addition to the problems of mineral decomposition during in-vacuo laboratory degassing, an equally important decomposition occurs during many hydrothermal experiments which, combined with problems of mineral purity, have led to an overestimation of the rate of argon diffusion in hornblende. The response of hornblende to thermal disturbance in a hydrothermal environment can be every bit as complex as breakdown in vacuo. Laboratory experiments on bulk samples have not succeeded in quantitatively constraining volume diffusion.

I.M. Villa (✉)
Universität Bern, Min. Pet. Inst; Gruppe für Isotopengeologie, Erlachstrasse 9a, CH-3012 Bern, Switzerland

B. Grobéty[1]
Johns Hopkins University, Dept. Earth Planet Sci., Baltimore MD 21218, USA

S.P. Kelley
Open University, Dept. Earth Sciences, Milton Keynes, MK7 6AA, UK

R. Trigila
Univ. Roma La Sapienza, Dip. Scienze della Terra, pza A Moro, I-00185 Roma, Italy

R. Wieler
ETH Zürich, Dept. Earth Sciences, Isotope Geology NO C61, CH-8092 Zürich, Switzerland

Present address:
[1] Geologisk Institut, Århus Universitet, DK-8000 Århus

Editorial responsibility: V. Trommsdorff

Introduction

In the early days of metamorphic geochronology, Ar loss from minerals was observed only as partial rejuvenation of K/Ar ages (Hart 1964; Hanson and Gast 1967), defined by the term "blocking temperature" (Jäger et al. 1967). The blocking temperature was simply the temperature below which the mineral retained argon quantitatively, as estimated from metamorphic petrology. With the introduction of the $^{39}Ar/^{40}Ar$ technique, pioneers (Berger 1975; Hanson et al. 1975) attempted to translate the model proposed by Turner (1968) for anhydrous, shock-metamorphosed meteoritic minerals to contact metamorphism of terrestrial minerals, including hornblende. The implicit hypothesis was that contact metamorphism had induced volume diffusion of Ar out of the crystals, and that the resulting concentric Ar zonation could be revealed by the stepwise heating since the latter also was believed to proceed by the same physical mech-

anism: volume diffusion. The model of Turner (1968) predicted a staircase-shaped age spectrum for a thermally overprinted hornblende. However, both Berger (1975) and Hanson et al. (1975) reported unexpected shapes of age spectra, which were to a large extent incompatible with this simplistic model.

Harrison (1981) argued that a staircase-shaped spectrum from a hydrothermally heated hornblende proved that a single diffusion mechanism operated during natural metamorphic conditions, $^{39}Ar/^{40}Ar$ in vacuo stepwise heating, and hydrothermal experiments. Thus, concentric argon gradients within mineral grains caused during natural or hydrothermal heating were indeed mirrored by the shapes of argon release spectra. However, Blanckenburg and Villa (1988) pointed out inconsistencies in the original database of Harrison (1981): resetting of contaminating biotite inclusions played an important role in the apparent argon loss. Further, Wartho (1995) has recently argued that many staircase-shaped spectra in both natural and laboratory heated samples not affected by biotite contamination have been caused by partial chemical re-equilibration and not by volume diffusive argon loss. Finally, in an exhaustive set of experiments, Lee et al. (1991), Wartho et al. (1991) and Lee (1993) have shown that in vacuo degassing proceeds by a series of breakdown reactions and not by volume diffusion.

Kelley and Turner (1991) re-addressed Ar loss using traverses of laser spot ages in contact-metamorphic hornblendes from localities near those studied by Hanson et al. (1975) and showed that Ar loss was associated with biotite grains forming along the cleavages, possibly during the same contact metamorphic event. Although Kelley and Turner (1991) attributed at least some of this loss to volume diffusion, Wartho (1995) has argued that potassium variations within the grains may be attributed to partial chemical re-equilibration.

This confused situation, in which the very foundations of Ar loss from hornblende have been explained by a range of sometimes mutually exclusive models, provided the stimulus for the present investigation. We report the comparison between four different $^{39}Ar/^{40}Ar$ experimental approaches: stepwise heating, IR laser spot fusion, UV laser depth profiling, and stepped etching, supplemented by TEM imaging of the experimental material.

While stepwise heating is useful to separate the Ar successively released from various phases and contaminants, recently developed alternative techniques allow the acquisition of complementary information. The infra-red $^{39}Ar/^{40}Ar$ laser microprobe is able to image spatial distribution of Ar with a resolution of ¥ 50 mm (Kelley and Turner 1987, 1991; Phillips and Onstott 1988) without any model-based assumptions; the UV-LAMP (Kelley 1994) has brought the depth resolution down to less than 5 mm. On the other hand, the observation that radiogenic ^{40}Ar ($^{40}Ar^*$) losses are correlated with HF-leachability via the density of extended defects (Villa 1990) suggests that gas release by closed system stepwise etching (CSSE; Signer et al. 1993) could be applied for $^{39}Ar/^{40}Ar$ dating of terrestrial minerals. CSSE has previously been been used to study depth profiles of the isotopic and elemental composition of solar noble gases in extraterrestrial samples (Wieler et al. 1986; Wieler and Baur 1994) and to selectively release a distinct primordial noble gas component residing in an HNO_3 soluble carrier in meteorites (Wieler et al. 1991). The basic idea of CSSE is to set free noble gases without having to subject the sample to high temperatures, thus assuring that diffusion does not play a crucial role in the gas release. Hence, CSSE should outperform stepwise heating for the separation of noble gas components residing in: (1) spatially distinct reservoirs, e.g., surface versus interior parts of grains; (2) domains of different etchability and possibly different noble gas retentivity, like lattice defects versus undisturbed crystal; and (3) inclusions or intergrown minerals. This is a desirable feature, since it is crucial that ^{40}Ar and ^{39}Ar atoms are analyzed in the same step if and only if they originate in the same site, i.e. if the distribution of the $^{40}Ar^*$ atoms is only related to the distribution of their parent K atoms. The realities of recoil (Onstott et al. 1995, and references therein; Villa 1996 submitted) indicate that there exists no sample for which the ^{39}Ar flawlessly reflects the K distribution. The situation is yet more complicated in the case of stepwise heating because of mass-dependent thermally activated diffusivity coefficients (Foland and Xu 1990). Furthermore, a prediction which might be testable by CSSE is that transport of Ar isotopes in the mineral lattice is independent of the location of origin of the particular atom after the first few lattice cells, as the rate-setting parameter is not the binding energy of the Ar atom to its site but the energy necessary to distort the lattice to let the Ar atom out to the surface (Villa 1991). If CSSE yields similar $^{40}Ar^*/^{39}Ar$ ratios to stepwise heating involving Ar transport, we may conclude that $^{40}Ar^*$ atoms which remained in the K lattice site and ^{39}Ar atoms which recoiled several lattice cells away from the parent K nuclei moved through the lattice following the same physical law. Villa (1991) argued that this law is the sum of the mobilities of all Ar-trapping defects.

Experimental techniques

The starting material for this study was a 400 g piece of the McClure Mountains syenitic intrusion, from which the international Ar-Ar dating MMhb-1 was separated. The geological context is sketched in Alexander et al. (1978) and references therein. This sample was not selected because of a mineralogical ideality, but because it represents a good example of the type of sample normally dated by Ar-Ar (Alexander et al. 1978; Samson and Alexander 1987), and in order to directly compare it with hydrothermal degassing results (Harrison 1981). From the whole rock we drilled out five 5-mm cores consisting mainly of hornblende aggregates. The cores were very gently handcrushed, and hornblende crystals with regular faces in the size range 0.5–2 mm handpicked. The sample thus prepared will be referred to as MMwr. The purpose of this separation was to obtain crystals large enough for a meaningful IR-laser traverse. A necessary compromise was the lower purity of MMwr compared to MMhb-1, whose distributed mesh fraction underwent a much more thorough mechanical separation; thin

sections of MMwr indeed showed a larger (¥ 4%) contamination by biotite. However, it will be seen later that this proved eventually to be an advantage. On the other hand, the biotite intergrowths are inhomogeneously distributed on the scale of our typical sample size, 10–15 mg. This caused some inhomogeneity in the calculated total $^{40}Ar^*$ concentrations of treated samples, but not on ages of the untreated crystals, for which biotite intergrowths yielded concordant step ages.

Half of the handpicked grains were irradiated without further treatment and are designated MMwr-C. Half the grains (designated MMwr-H) were treated at 846 °C, 200 Mpa (2 kbar), for 96 h in a hydrothermal high pressure apparatus with externally heated vessel (Dolfi and Trigila 1988), and irradiated. From the standpoint of experimental petrology, the design of the present bomb run may initially appear not to be optimal. Among the various parameters controlling the reactions in the experimental capsule, we only monitored P, T, f_{O_2} and X_{H_2O}. However, it should be noted that this has been the common practice in geochronology-based diffusion experiments (e.g. Harrison 1981) and this did not result in lower quality experiments than others found in the literature, nor in pervasive degradation of the hornblende (see later), probably because there was only one major mineral phase in the capsule charge.

The hydrothermal treatment comminuted the sample: most of the heated grains were 10–30 mm, but a few individuals up to 1 mm long survived intact, probably due to a sheltering mechanism similar to that observed during in-vacuo crushing by Dunai et al. (1992). Samples of each grain population were allocated to the different $^{39}Ar/^{40}Ar$ experiments. A few dozen grains of each were mounted in plaster of Paris ($CaSO_4$) without further polishing for the IR laser microprobe traverses (procedures in Kelley and Turner 1991) and UV laser depth profiles (Kelley 1994), while ¥ 10 mg unmounted grains were used for stepwise heating analyses (procedures in Villa 1992) and closed system stepped etching. This latter technique is slightly modified relative to Signer et al. (1993) in which noble gases were released by etching samples in an ultra-high-vacuum extraction line connected directly to a noble-gas mass spectrometer. In the present work a miniaturized line was used in which acid-exposed parts including valves consist exclusively of pure gold or platinum (Signer et al. 1993). Samples are exposed first to the vapours of an etchant, in this case 28N HF, previously degassed of all air. Only in the last few steps of each run was acid distilled onto the sample to enhance the etching speed. Etching times increased from 10 min in the first steps to up to three days towards the end of a run, with acid temperatures increasing from a few degrees below 0 °C up to room temperature. When the gases of a step were expanded into the purification line, the HF was kept at −20 °C to reduce its vapour pressure and thus the HF amount to be digested by the getters (CaO powder, followed by ZrTi and ZrAl). The signal at mass 19 did not increase significantly when a sample step was admitted into the spectrometer, indicating very efficient clean-up. Previous experience and tests during the present analyses showed that no substantial fraction of the Ar liberated in a given step was retained in the extraction part of the line, e.g., dissolved in the acid. The possibility that Ar was partly bound as ArF_2 can also be excluded.

The very significant increase of etching times as well as acid temperatures in the course of the runs, which were necessary to keep the Ar amount per step at a roughly constant level, can only partly be attributed to the fact that more easily etchable phases are etched first. Most probably, in later steps fluoride layers protected the grains to some degree from the HF vapour. The etching efficiency of the small amounts of liquid acid that were transferred onto the sample prior to step 9 of the first run of sample C was underestimated, such that nearly all the remaining 70% of the Ar was liberated in this single step. A duplicate experiment on sample C was thus performed. Mass spectrometric analyses were performed as described by Wieler et al. (1989) and Graf et al. (1990). The mass spectrometer used for these analyses has acquired a rather high ^{36}Ar memory from analyses of lunar soil samples with $^{36}Ar/^{40}Ar$ values close to unity. This causes a somewhat imprecise correction of the measured ^{40}Ar for atmospheric contributions. The uncertainty is such that $^{40}Ar/^{36}Ar$ ratios in the gas-poor steps 1 and 2 of run H with a nominal value of 302 may actually be not significantly above the atmospheric ratio of 295.5. However, all steps with substantial Ar amounts show highly radiogenic $^{40}Ar/^{36}Ar$ ratios mostly above 1000. The imprecise correction for atmospheric ^{40}Ar has a very minor influence on the radiogenic ^{40}Ar.

For the artificial mixture experiment, the age standard MMhb-1 was mixed with a Miocene granitic K-feldspar, GA-1 (Villa 1994), in a mass ratio 1.02:1 to ensure visible effects.

TEM observations were performed for both the untreated and the treated hornblende. Two 2.3 mm discs cut from a petrographic thin section of chips of the MM whole rock containing hornblende were mounted on a copper grid, ion-milled and coated lightly with carbon. Thin edges representing both the rims and the interiors of several grains were present in both discs. An aliquot of the hydrothermally treated sample MMwr-H was suspended in acetone and gently ground in an agate mortar. The powder was then deposited on a carbon-coated copper grid. Electron microscopy was performed with a Philips 420ST microscope operated at 120 kV, and a 50-mm objective aperture was used for high resolution experiments. Semiquantitative chemical analyses were performed with an energy dispersive spectrometer linked to the microscope column (Livi and Veblen 1987).

Finally, SEM observations were performed on unirradiated grains of MMhb-1 (Alexander et al. 1978) that had been exposed to HF vapours at room temperature and atmospheric pressure. In addition to images, the CamScan Series 5 SEM provided us with semi-quantitative EDS spectra on selected reprecipitated fluorides.

Results

Microscopy

Control sample

The microstructure of the untreated MMwr-C sample is characterized by dislocations, cleavage planes and micro-inclusions. The dislocation density is patchy and ranges from 10^2 to 10^8 cm^{-2}. There is no evident relationship between dislocation density and the location within the grain or other microtextural features. Planar defects are homogeneously distributed throughout the grains and are generally parallel to the {110} cleavage or the basal plane. Most of the cleavage planes are filled by either biotite or more often feldspar, both albite and alkali feldspar (Fig. 1a, b). Rare muscovite and chlorite also occur. The filling of the cleavage planes indicates that the defect is natural and not due to sample preparation. Biotites and feldspar intergrowths may be of magmatic origin indicating that the cleaving occurred very early in the history of amphibole; indeed, melt-filled cleavage planes have been found in pyroxenes from New South Wales (Mellini and Cundari 1989). A second type of planar defects (//{110}) is characterized by very narrow, amorphous layers (<2 nm). The amorphization of such material is most likely an artefact of the ion milling technique and is commonly observed in TEM analysis. It is difficult to determine whether the {110} cleavage planes without fillings formed naturally or during sample preparation. Dislocations are often found at the origin of these planes (Fig. 1c). The separation of all {110} cleavage planes, filled or unfilled, ranges from <1 mm to

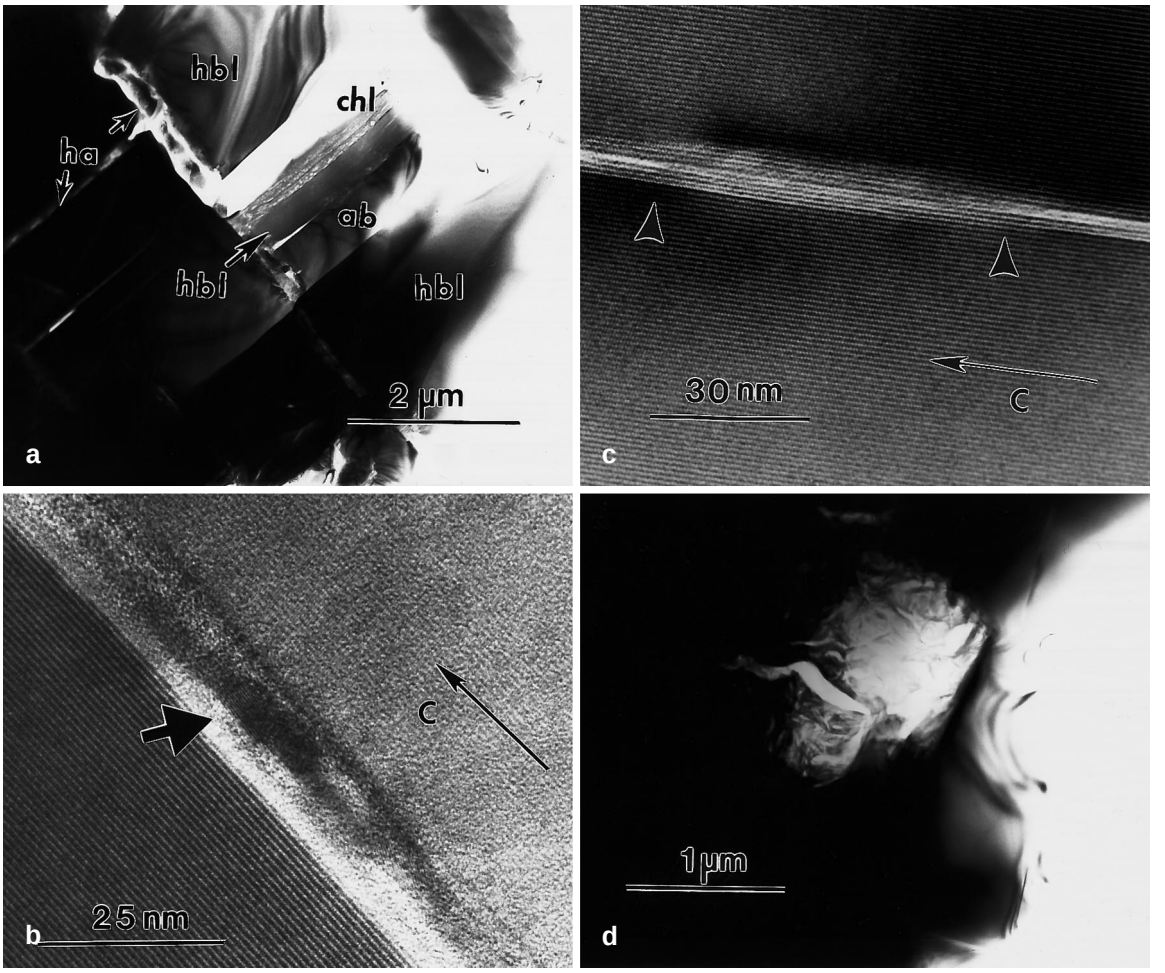

Fig. 1a–d TEM images of MMwr-C hornblende. **a** Ion-thinned edge of a region close to the core of a hornblende (*hbl*) grain. Two sets of cleavage planes are visible, one parallel to (001), the second one parallel to (110). The cleavage planes are filled with halloysite (*ha*), chlorite (*chl)* and albite (*ab*). The density of filled fractures seen in this image is much higher than the average density. The distances between them are one order of magnitude smaller than elsewhere in the grain and not representative for the bulk sample. **b** [310] HRTEM image of hornblende with a cleavage plane running parallel to the *c*-axis. Within the gap a second set of lattice fringes of an unidentified phase is visible (*arrow*). **c** [310] image of hornblende showing two dislocation cores (*arrows*) from which two cleavage planes start. **d** Spheroidal inclusion filled with halloysite

150 mm (measured along {110} or {$\overline{1}$10}). The separation of the basal cleavage planes, which are mostly filled, is very irregular (10–500 mm). The MMwr hornblende (as seen in the TEM) can, therefore, be represented as composed of {110} {001} prisms of different sizes and with a large variation in aspect ratio.

The minerals filling the cleavage and probably also hornblende are partially altered to an ill-crystallized phyllosilicate, which forms also spherical inclusions within the hornblende (Figs. 1a, d). The irregular, curly shape, the chemical composition (no alkalis) and the electron diffraction pattern (1 nm basal reflections) are typical of halloysite, a kaolin-group mineral with water in the interlayer. Halloysite is a low-temperature alteration product of a variety of silicates (Giese 1988). Other small mineral inclusions include monazite and titanite grains. The total amount of impurities on the submicron scale is 0.5–1%, though this value does not take into account the coarse, optically visible biotite inclusions.

Heated sample

The fragments of the hydrothermally treated hornblende did not have sufficient electron-translucent edges and needed to be crushed further. This treatment destroyed microstructural information, since the grain broke preferentially along weak boundaries. Chemical analyses and electron diffraction from the grains show that the powder still consists of hornblende. The composition and the lattice parameters underwent no changes within the resolution of the electron diffraction method; i.e. the hornblende remained stable during the hydrothermal treatment. The same is valid for biotite. Feldspar relics were also present in sample MMwr-H.

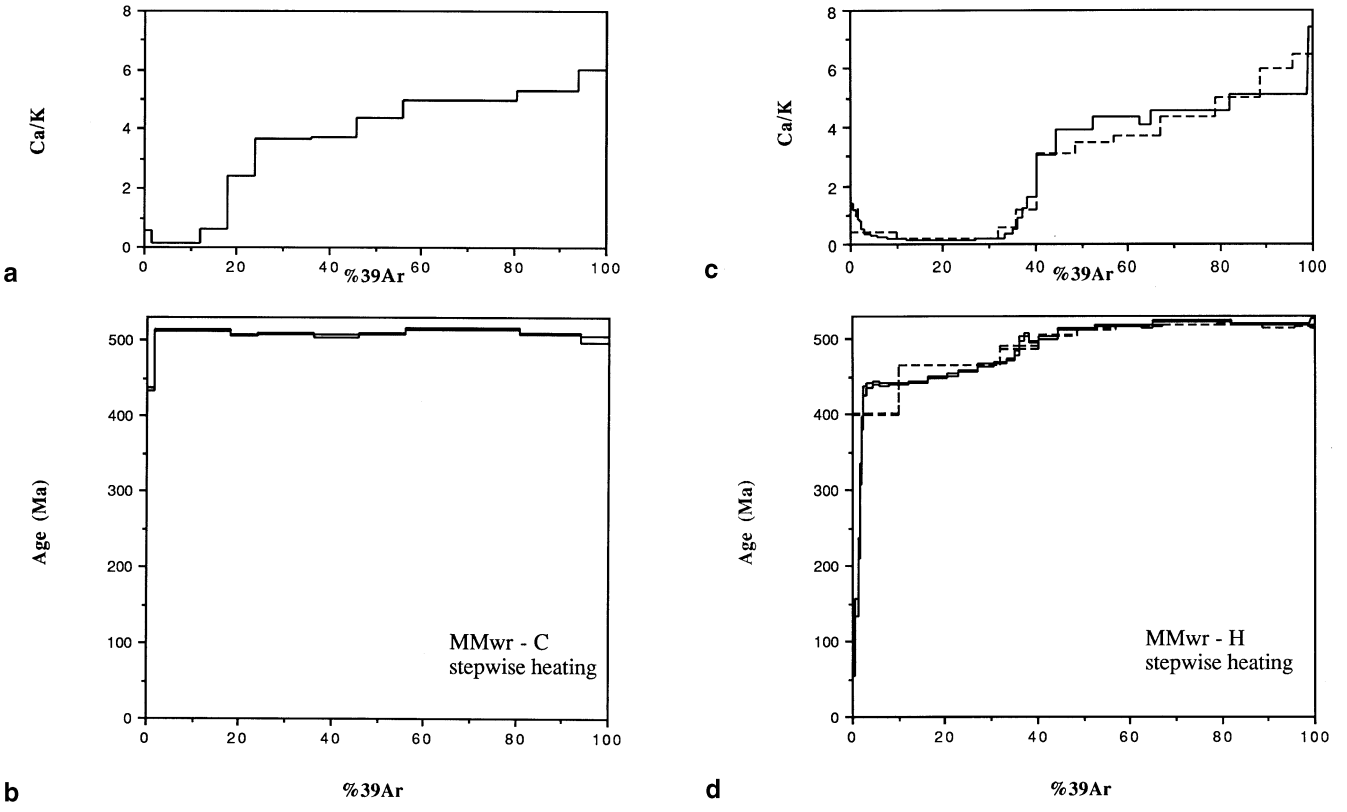

Fig. 2a–d Stepwise heating spectra. **a** Ca/K and **b** age spectrum of the control sample MMwr-C; **c** Ca/K and **d** age spectra of duplicate runs H1 and H2 of the heated sample MMwr-H

Stepwise heating

The stepwise heating results set the baseline for the interpretation of the other experiments. Three runs were performed: one on the control sample, MMwr-C, and two on the heated one, MMwr-H.

The spectrum of MMwr-C is flat (Fig. 2b), with a 9-step plateau containing 98% of the gas. An important observation is that the steps containing a high proportion of biotite-derived Ar (i.e. in early steps, as revealed by the Ca/K spectrum: Fig. 2a) are the same age as those deriving from "pure" hornblende (Ca/K > 3).

The spectra of the two heated samples are very similar (Fig. 2d) and resemble that reported by Harrison (1981). The effect of the comparatively abundant biotite intergrowths is to make clearer the correlation between low Ca/K portions of the release spectrum (Fig. 2c) and low step ages. The portion of the spectrum with Ca/K > 3 has an age of 515 Ma, relative to a 520.4 Ma age for the MMhb-1 standard (Samson and Alexander 1987).

The total Ar loss, F, in the two bulk H aliquots is similar (6.8 and 7.3%). If this figure were taken to solely reflect Ar loss from hornblende, one would derive diffusivities $D(846\,^{\circ}C) = a^2 * (F^2 * t)/36\,p = (1.9-2.2) \cdot 10^{-14}\ cm^2 s^{-1}$, respectively (for an estimated average grain radius of 40 mm), which is higher than the literature value (Harrison 1981). If, however, the biotite contamination is subtracted based on the Ca/K ratio of each step, the Ar lost from the steps with Ca/K > 3 is F = 1.8 and F = 1.3% for the two aliquots. Diffusivities D(846 °C) are thus 13 and $6.5 \cdot 10^{-16}\ cm^2 s^{-1}$, an order of magnitude lower than the literature value (Harrison 1981).

To illustrate the role of sequential breakdown of mineral separates during in-vacuo heating, we performed a stepwise heating experiment on an artificial mixture. Artificial mixtures are a powerful tool to understand the degassing behaviour of natural impure minerals (see Wijbrans and McDougall 1986; Rex et al. 1993). Because our electron microscopy had revealed ubiquitous, minute K-feldspar in the McClure Mountains hornblende, it appeared possible that the contrasting Ar signature of these two minerals could be responsible for the reproducible, statistically well-resolved deviations from a plateau in MMhb-1 (Lee et al. 1991, Fig. 2; this work, Fig. 2b; see Harrison 1981, Fig. 2, where the deviations are not significant due to the high errors).

The stepwise heating age spectrum (Fig. 3a) shows a double hump shape, with hornblende having the greatest relative weight in the middle temperature steps and K-feldspar both at lowest and at highest temperatures. While at the scale of Fig. 3a MMhb-1 and GA-1 both define a "plateau", their mixture clearly does not, and exhibits precisely the sort of oscillation that we are trying to explain.

The artificial mixture further helps to illustrate the behaviour of binary systems in three-isotope correlation plots. The two pure end-members MMhb-1 and GA-1 are shown in Fig. 3b (a Cl/K vs Ca/K correlation plot) and

Fig. 3c (an $^{40}Ar^*/K$ vs Ca/K correlation plot). The total gas release of the mixture is coincident with the mass balance calculation. It can be seen that all steps except the first ones are well aligned in Fig. 3b, c. It is very likely that the imperfections in the alignment stem from the fact that neither "pure" end-member is really ideal, but rather each is a normal geological mineral separate containing a variety of small inclusions.

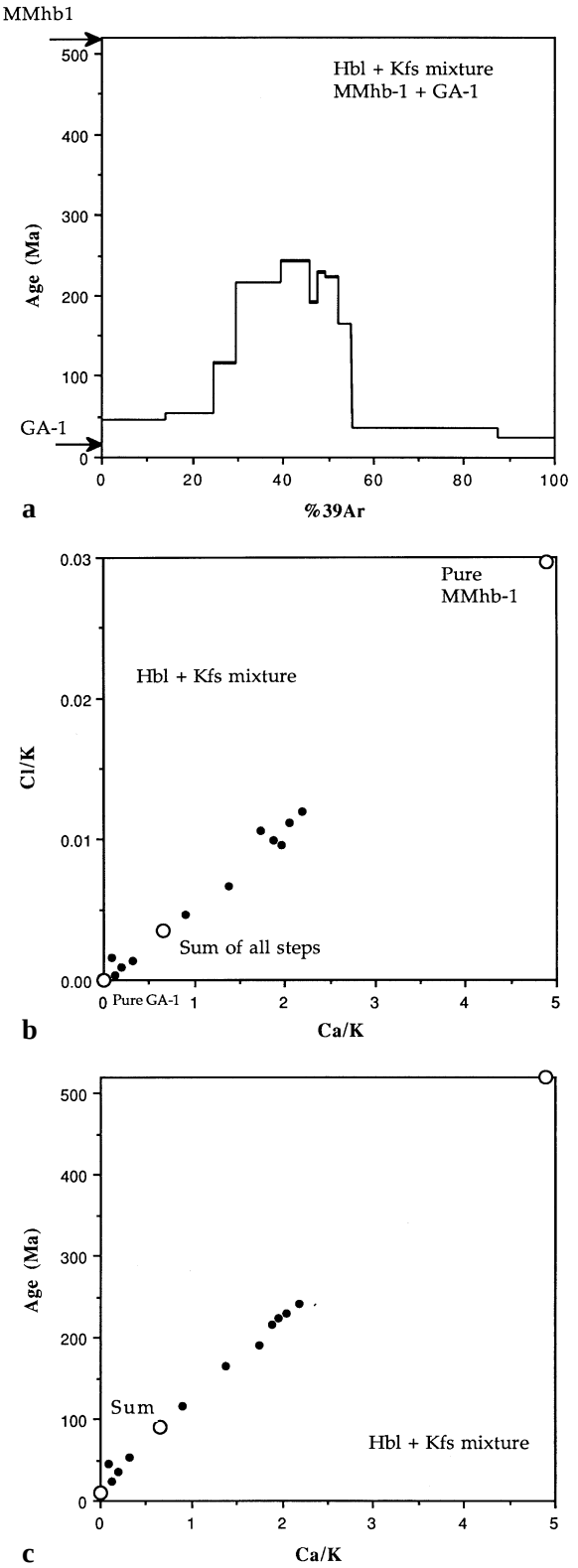

IR Laser microprobe

The traverse of the control sample, MMwr-C, yielded constant ages within experimental error. One grain yielded a low Ca/K ratio and was certainly contaminated by biotite, though the resulting age was indistinguishable from the others.

A traverse across a large heated grain from MMwr-H, around 900 mm diameter, yielded ages indistinguishable from the untreated sample (Fig. 4a), even at the margins. One point falls slightly below the mean of the control sample, but the difference is less than 2s (Fig. 4a). However, as Ar loss undoubtedly occurred from the bulk sample, mass balance requires that some grains show some rejuvenation. We thus proceeded with a survey of 29 single grain fusions on the MMwr-H fraction. The analyses, shown in Fig. 4b, show a range of fractional losses only vaguely correlated with the measured grainsize (measured using the XY stage of the microscope). Single grains were analyzed where possible, though of the smaller grains two or more of similar size were analyzed. If the Ar loss during the hydrothermal treatment had been the result of volume diffusion from hornblende, the proportions of fractional loss should correspond to the dashed line in Fig. 4b. Clearly, although some of the points fall close to the line, many fall below. This may be due to contaminating biotite grains (see earlier). Although the ^{37}Ar had largely decayed prior to these analyses, using the measured grain size and the sensitivity of the mass spectrometer, several analyses yielded ^{39}Ar corresponding to potassium contents higher than the known potassium content of MMhb-1 (Samson and Alexander 1987).

In summary, the infra-red laser microprobe results from a single hydrothermally treated, unaltered grain show no evidence for Ar loss at the physical grain boundaries, although, given the experimental parameters, argon loss would only have occurred in the outer 2–3 mm of grains. Analyses of smaller grains yielded very variable amounts of Ar loss, generally greater than that predicted from existing experimental data on bulk hornblende (Harrison 1981; Baldwin et al. 1990). This

Fig. 3 **a** Stepwise heating spectrum of an artificial mixture between hornblende age standard MMhb-1 (520 Ma) and K-feldspar GA-1 (20 Ma). While both pure minerals have flat spectra at this scale, their mixture shows an irregularly discordant spectrum. **b** Three-isotope correlation plot (converted to chemical element ratios) showing the linear trajectory resulting from simple binary mixing. Note that the sequence of the individual heating steps is erratic as a result of differential breakdown, but the linear trend preserves the information on the mixing. **c** Three-isotope correlation plot (converted to age vs. element ratio), essentially analogous to **b**. The apparent disorder of the age spectrum in **a** is clearly seen to result from a linear mixing trend of two distinct phases

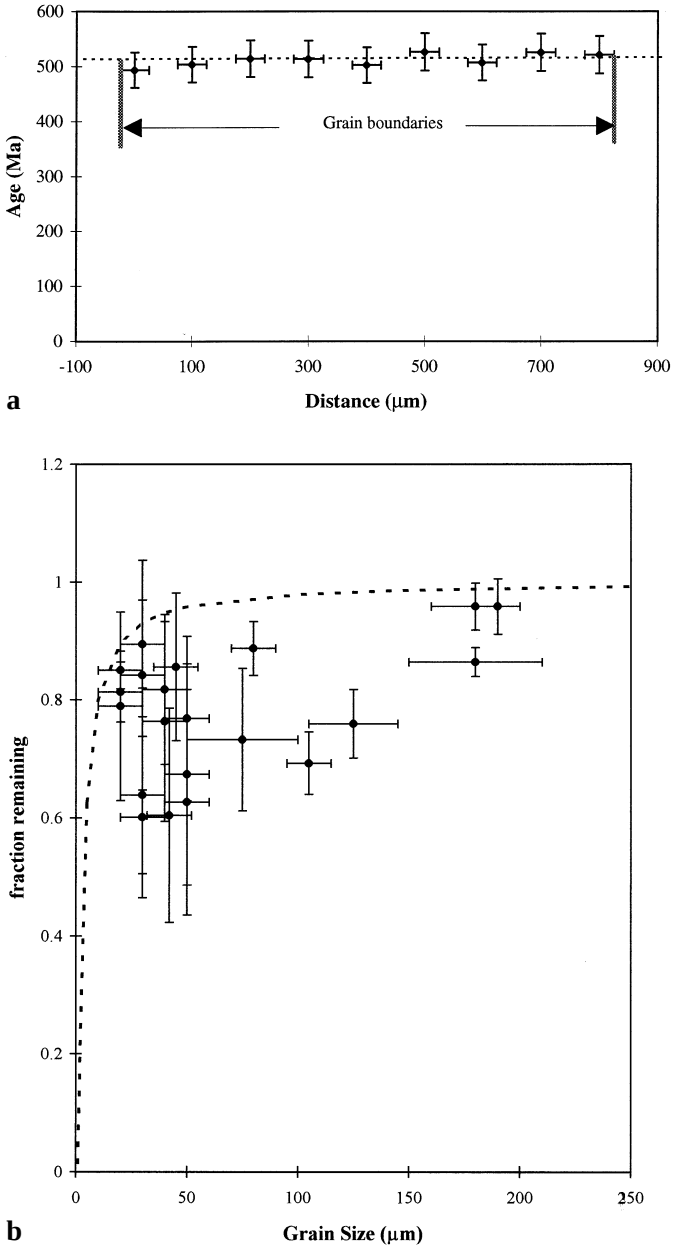

Fig. 4a, b IR laser experiments. **a** Age traverse of a single grain 0.9 mm across. *Dashed line* is the reference age for MMhb1 (520.4 Ma). **b** $^{40}Ar^*$ fraction remaining in MMwr-H single-grain fusions (relative to the age of MMwr-C) as a function of grain size. The *dashed curve* depicts the grain-size dependence of volume diffusive loss of Ar during hydrothermal treatment (see text)

replicates the result of the stepped heating which indicates biotite as the main culprit for the Ar loss. While the high ^{39}Ar concentrations are indirect evidence for the presence of a K-rich contaminant, the dichotomy of the $^{40}Ar^*/^{39}Ar$ ratio in the heated aliquot H between the large grain showing no loss (Fig. 4a) and the numerous small grains showing erratic losses (Fig. 4b) cannot be explained other than by a heterogeneous phase population. The much higher proportions of loss exhibited in the laser experiments reflect true variation whereas the stepped heating experiment produced a mean value caused by the vacuum breakdown of the mineral (Gaber et al. 1988).

UV laser microprobe

An experiment using a UV laser microprobe (Kelley 1994) analyzed the hydrothermally heated sample to determine the depth distribution of the atmospheric ^{36}Ar introduced during the bomb run.

A fresh cleavage surface was created in a grain and two adjacent depth profiles were analyzed from the new surface. The grain is illustrated after the laser ablation experiments (Fig. 5a, b). Both profiles were analyzed using 100 mm square rastered pits (see Kelley 1994) and thus to obtain sufficient Ar for analysis, the resolution was around 6 mm (resolution calculated from ^{39}Ar release during each analysis). The variations of $^{36}Ar/^{39}Ar$ ratios of the two depth profiles are very similar (Fig. 5c), starting at low values close to the newly created surface, followed by an excursion to higher values at 30 mm depth, a return to low values at around 40 mm, and slow increase to the base of the pit. Clearly, the grain contained features which parallel the mineral cleavage traces and carry high proportions of atmospheric Ar. This observation is readily explained by the TEM observations, since the clay mineral halloysite which fills many cleavages contains neither K nor Ca and would thus have no effect on the Ca/K ratio, while contributing large quantities of atmospheric Ar (monitored by the ^{36}Ar isotope), acquired from water in the hydrothermal bomb. It also demonstrates the presence of fast pathways for Ar through apparently unaltered grains of the mineral at a scale of a few to a few tens of microns. Averaged over a whole grain, such an effect might explain the difference between estimates of the effective grain size for Ar diffusion between laboratory experiments (Harrison 1981) and laser microprobe analyses of natural samples (Lee et al. 1989; Kelley and Turner 1991) and underscores the fact that, at least in the case of hornblendes, modelling natural minerals by laboratory experiments may raise as many problems as it solves.

Stepwise etching

The two etch age spectra of the untreated sample, C, are similar to each other (Fig. 6b). Since 70% of the Ar was inadvertently released in a single step in run C1 and no Ca/K data are available from this run, we concentrate on C2. There are some small but important differences between the age spectrum of this sample and that of the respective heating run. The first four etch steps, representing the first 5% of the gas, have apparent ages clearly below those of the later steps, contrasting the step-heating data, which give a near-perfect plateau for sample C. The age of etch step 1 is also below the anomalously low value of the first heating step and also corresponds to the

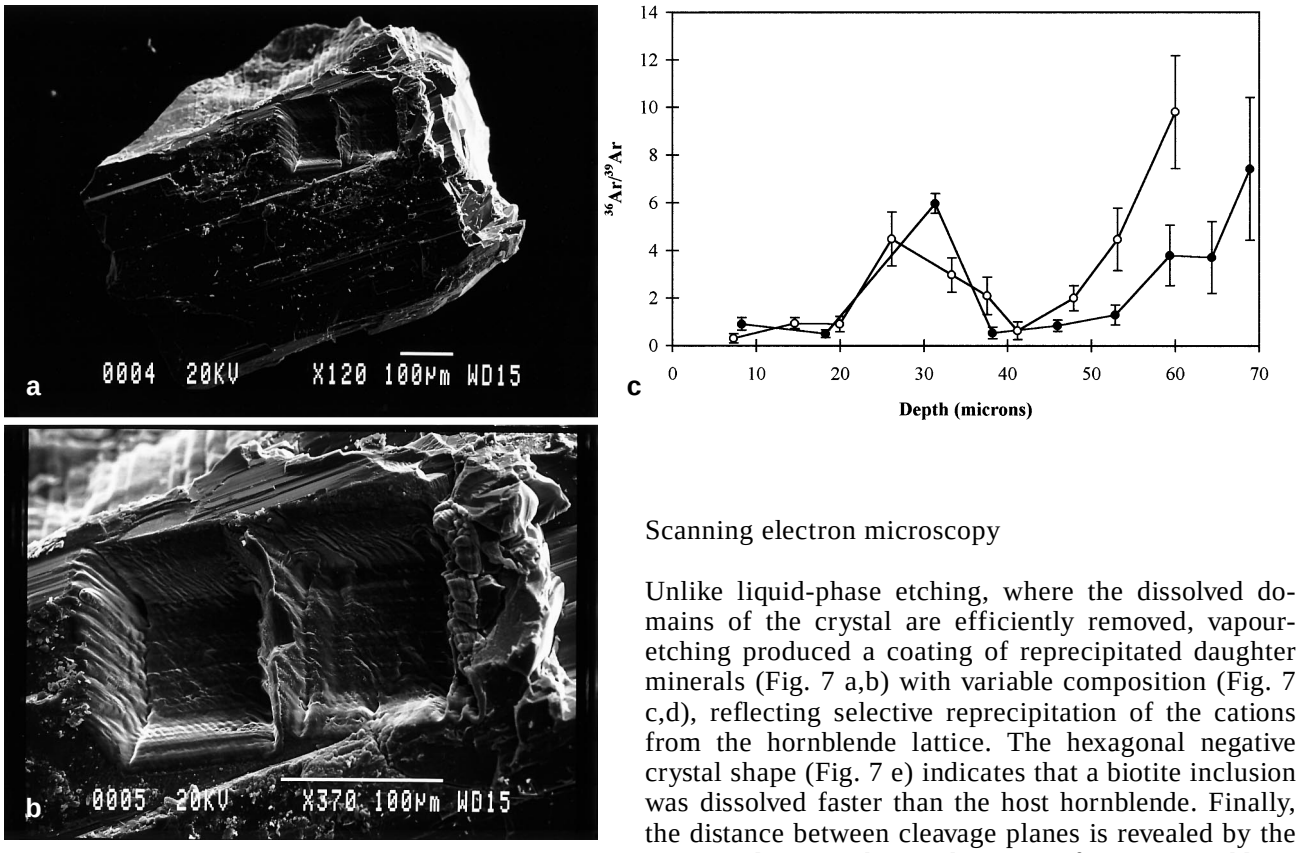

Fig. 5a–c UV laser depth profiles. **a**, **b** SEM photographs of laser pits on freshly cleaved hornblende. **c** $^{36}Ar/^{39}Ar$ ratio measured in these pits, as a function of pit depth

lowest Ca/K ratios (Fig. 6a). Natural Ar loss from minerals with a low Ca/K ratio was thus revealed by the stepped etching of the untreated sample, an effect not obvious from the step-heating data. The two different methods also yield slightly different age patterns in the later steps. Contrasting the plateau displayed by the stepwise heating run, the apparent ages in the etch run increase slowly but monotonically and reach the highest value in the last two steps (two very gas-poor steps with large errors being ignored). We shall return to this point in the discussion.

For sample MMwr-H, the apparent age patterns of etching and stepwise heating runs are very similar (Fig. 6d). Low ages show up in the first 30–40% of the ^{39}Ar release and nearly constant apparent ages are to be observed during the remainder of the runs. The first steps display low Ca/K ratios (Fig. 6c), clearly indicating minerals other than hornblende as the main culprits for the low apparent ages. This very important observation means that both stepwise heating and etching have tapped Ar from different mineral phases having different Ar retentivities at different times from the Ar contained in the bulk of the hornblende. Closer examination reveals important differences between etching and stepwise heating: the steps with high Ca/K display an age plateau in the latter but still slightly increasing ages in the CSSE.

Scanning electron microscopy

Unlike liquid-phase etching, where the dissolved domains of the crystal are efficiently removed, vapour-etching produced a coating of reprecipitated daughter minerals (Fig. 7 a,b) with variable composition (Fig. 7 c,d), reflecting selective reprecipitation of the cations from the hornblende lattice. The hexagonal negative crystal shape (Fig. 7 e) indicates that a biotite inclusion was dissolved faster than the host hornblende. Finally, the distance between cleavage planes is revealed by the incipient linear etch troughs (Fig. 7 f). We were able to confirm the observation by Berner (1981, p. 125) that it is of the order of 1 µm.

Discussion

The combination of these four rather different $^{39}Ar/^{40}Ar$ techniques with the hydrothermal experiment allows us to discriminate between two possible argon diffusion scenarios both in the present hydrothermal experiment (with low Ar loss) and in geological environments (where Ar loss can exceed 50%).

1. Thermally overprinted hornblendes lose $^{40}Ar^*$ by volume diffusion, resulting in concentric zonation within individual grains (Fig. 8a). This model predicts the following results on a large crystal (say 1 mm) with three of the employed techniques. Stepwise heating should reflect the concentric gradients via a staircase shape, corresponding to approximately constant Ca/K ratios (Fig. 8c), which may be deconvoluted using an effective grainsize for diffusion, a_{eff} = 80 + 20 µm (Harrison 1981). Laser microprobe spot fusion would resolve individual diffusion domains (about 3×3 are contained in a 0.5×0.5 mm crystal), in the form of a a sinusoidal age traverse (Fig. 8e). Finally, etching is known to initiate along extended defects (MacInnis and Brantley 1993), principally of all planar defects cutting across hornblende crystals with spacings <10 µm (Berner 1981; Lee 1993). The predicted age spectrum of the CSSE experiment is therefore a subdued staircase (Fig. 8g), in which

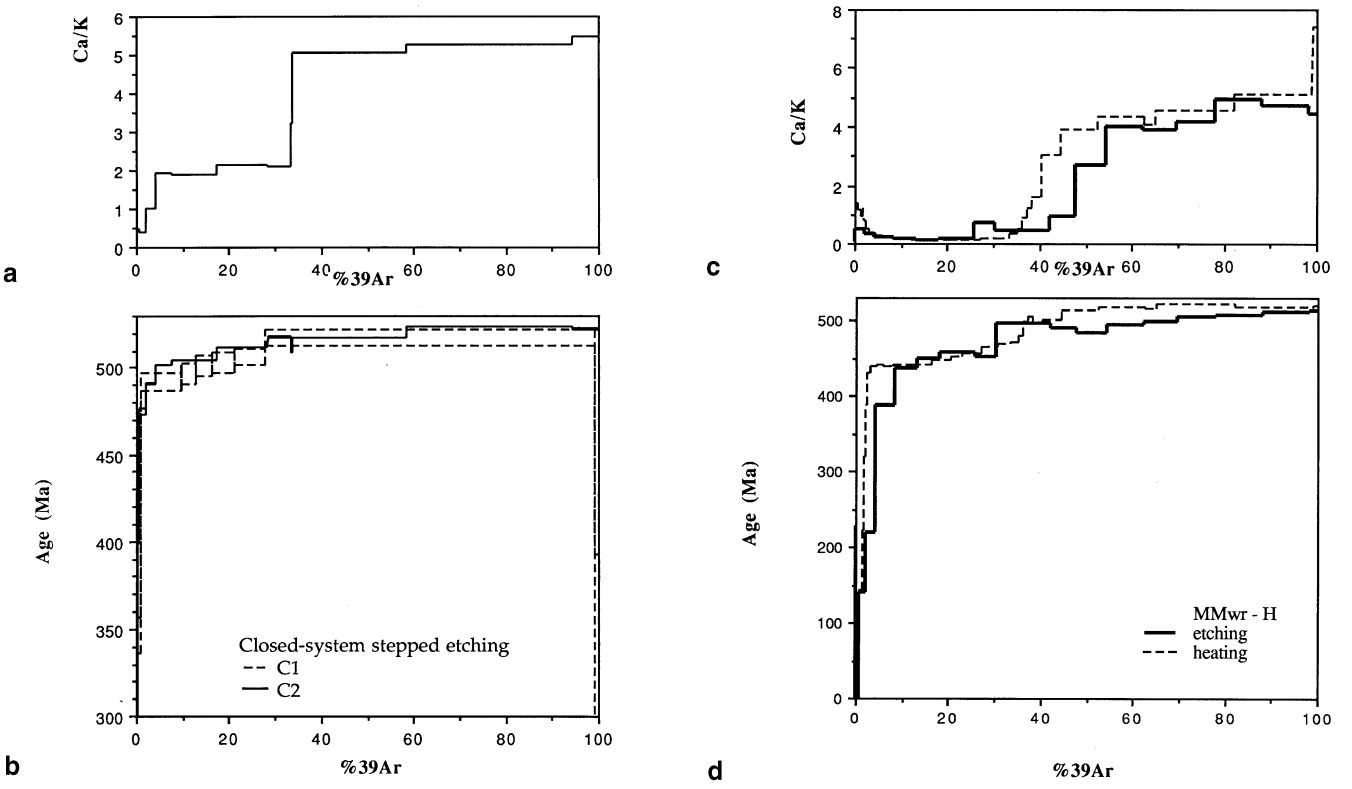

Fig. 6a–d CSSE spectra. **a** Ca/K spectrum of C2, **b** age spectra of duplicate measurements C1 and C2 of control sample MMwr-C. **c** Ca/K and **d** age spectrum of heated sample H (*solid line*) compared with the stepwise heating run (from Figs. 2c--d)

the age of the initial release steps is a mixture between young rim ages and the older ages of the 80 mm radius "domain" cores which are attained by the defect-assisted etching.

2. Argon loss is initially dominated by loss from fine-grained impurities and via fast channels (e.g. planar defects; see also Lee 1993); volume diffusion from the hornblende lattice proper becomes important only at high fractional losses (Fig. 8b). The predictions made for the outcomes of the three experiments on the thermally perturbed hornblende are also sketched in Fig. 8. The stepwise heating age spectrum (Fig. 8d) will comprise three sections: fine-grained impurities and zones rich in fast pathways which lose Ar easily (both $^{40}Ar^*$ during the thermal disturbance and ^{39}Ar during the first steps of the in vacuo-heating) and the Ca/K ratio should be erratic; below ©1050 °C, biotite and feldspars with strongly reset ages and a characteristically low Ca/K ratio dominate the release. The amphibole lattice which dominates the release between 1050 and 1200 °C shows only minor resetting; feldspar contributions are again visible in the highest temperature steps. The laser traverse should also show an essentially flat trend except for sudden drops where fine-grained impurities (biotite, feldspars) and/or zones rich in fast pathways are included within the analysis (Fig. 8f). Finally, the CSSE should yield zero ages at the beginning of the release (the porous fine-grained impurities observed under TEM have a very large and embayed surface per unit volume, enhancing etchability); the middle section depends on the relative HF solubility of impurities and hornblende; our observations suggest that impurities are dissolved first (Fig. 7e), so that amphibole will be the only phase left towards the end of the run.

The argon isotope results for stepped heating, IR and UV laser analysis and CSSE, presented in Figs. 2–6 are not compatible with the model sketched in Fig. 8a; the more complex model in Fig. 8b represents a better working hypothesis. The staircase-shaped age spectra do not mirror a concentric Ar zonation, but represent the superposition of three effects which take place at different crucible temperatures: Ar loss via fast diffusion pathways; degassing by breakdown of fine-grained biotite and feldspar intergrowths; and breakdown and degassing of hornblende. However, the results from the range of analytical techniques employed here now give us a clearer understanding of the processes than was possible in the past.

The present experiment may also shed light upon the relationship between in-vacuo release of argon and possible natural argon concentration profiles in the MMwr sample. It is interesting to note that in other sample suites where diffusive argon loss is a priori thought to have occurred, problems have been encountered in relating the natural concentration profiles to release spectra. The argon concentration profiles measured by Kelley and Turner (1991) on a contact-metamorphozed hornblende seem to translate into the staircase-free pseudoplateaus

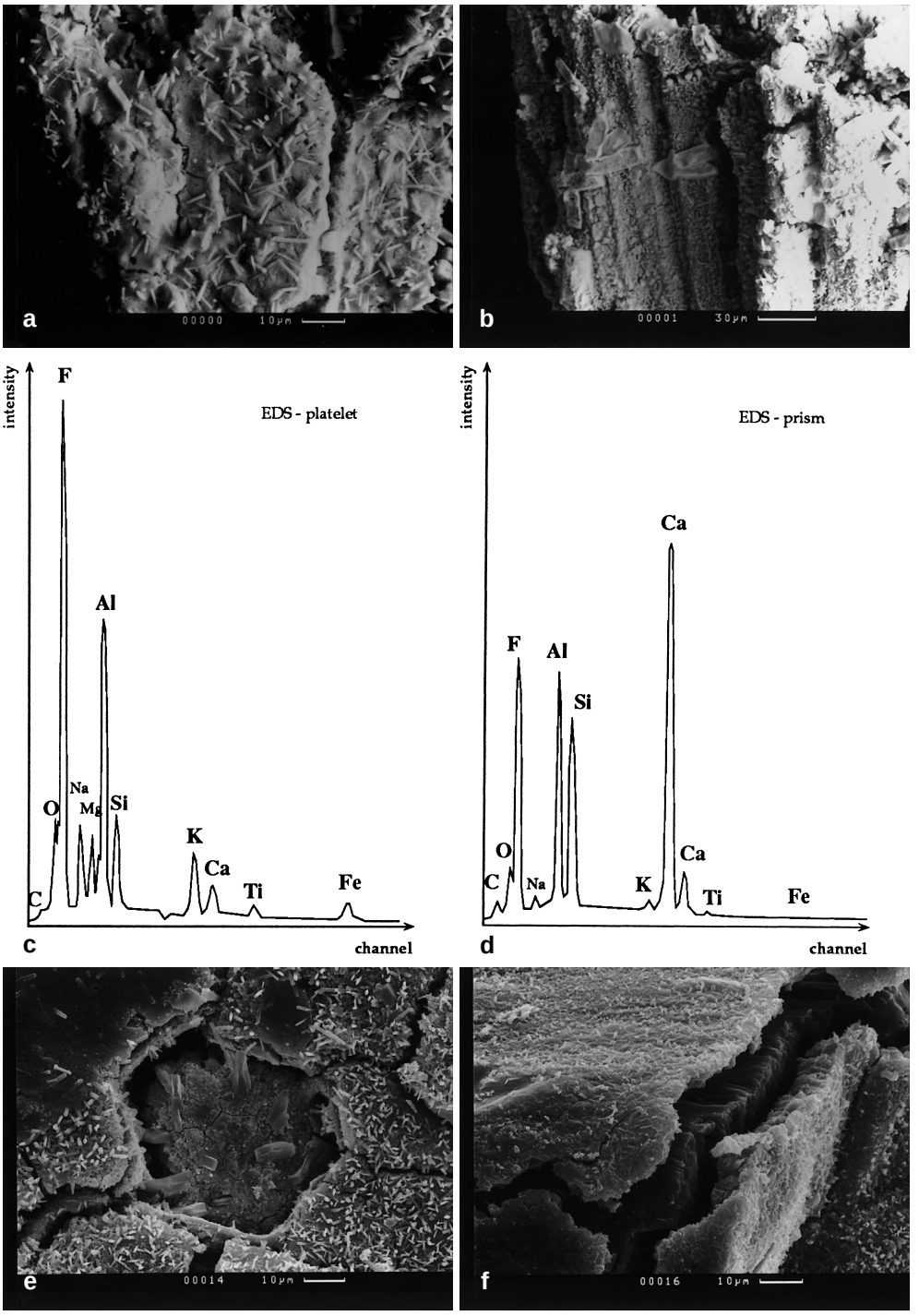

Fig. 7a–f SEM images of vapour-etched MMhb-1 hornblende grains. **a, b** Grains etched for 30 min at 20 °C. The surface is coated by a white, cracked coating, consisting of a microcrystalline layer 10–50 mm thick decorated by needles, platelets and prisms. **c** EDS spectrum of platelets shown in **a**. **d** EDS spectrum of prisms shown in **b**. **e** Negative crystal, possibly a dissolved biotite inclusion. **f** Grains etched 10 min at 20 °C. The white crust is cracked at the edge, exposing the undissolved hornblende core which displays incipient etch troughs spaced 1–2 mm.

obtained by Berger (1975) and combined plateaus and biotite contamination measured by Hanson et al. (1975) on a very closely related sample suite. Moreover, two texturally distinct hornblende samples from the same hand specimen yielded statistically acceptable but distinct plateaus, interpreted as excess Ar (Blanckenburg and Villa 1988). These features are reminiscent of the behaviour of biotites. Berger (1975) and Foland (1983) showed that biotite plateau ages may hide either a rejuvenation or excess Ar. This characteristic derives from the dehydration of the lattice below 1000 K, which homogenizes any spatial distribution of isotopes (Gaber et al. 1988; Phillips 1991).

A different kind of spectrum is sometimes found in samples which are a priori expected not to have been overprinted. As noted, the age standard MMhb-1 has a reproducibly discordant spectrum. The diagnostic properties of the Cl-Ca-K-Ar correlation diagrams (Fig. 3) can be exploited to examine the phase mixtures composing MMhb-1 (and a fortiori MMwr) as well as to com-

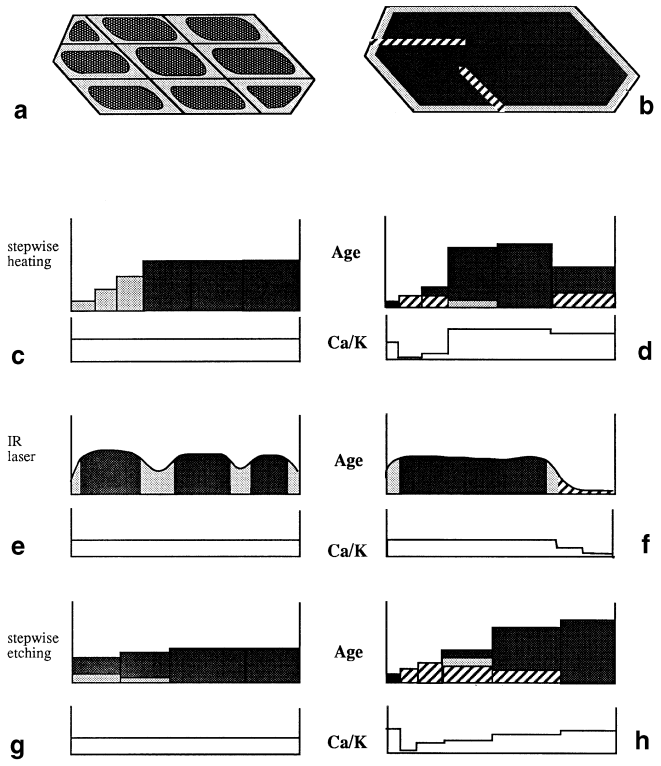

Fig. 8a–h Idealized Ar distributions of thermally overprinted hornblende predicted by different interpretive models. *Left column* (model 1): **a** hornblendes consist of a mosaic of concentrically zoned 80 mm "domains"; the patterning is therefore rendered by simple light-dark tones reflecting large and small diffusional losses, respectively. Its stepwise heating age spectrum **c** should be a staircase; its IR laser age traverse **e** a sinusoidal curve, and its CSSE spectrum **g** a subdued staircase, all with a roughly constant Ca/K ratio. The sinusoidal pattern in **e** is due to large fractional Ar losses typical of geological environments (e.g. Kelley and Turner 1991). *Right column* (model 2): **b** Hornblendes are multiphase assemblages which lose Ar in-vacuo first from fast pathways distributed over the entire crystal (*black pattern*), then by sequential breakdown of mineral impurities, shown by *dotted* and *hatched* patterning for hornblende and biotite + feldspars, respectively. *Light dotted pattern* at the grain rim denotes a narrow zone where volume diffusion from hornblende proper may have occurred. **d** The stepwise heating age spectrum will show a correlation between age and Ca/K ratio; note the release of Ar from feldspars at high temperature (*hatched pattern*). **f** The IR laser traverse should be flat in areas of constant Ca/K ratio (hornblende *sensu stricto*, with possible minor influence of volume diffusion shown by *light dotted pattern*), but will show large variations when extraneous phases are melted. **h** The importance of extended and planar defects for both diffusion and etching should be mirrored by a close similarity of the initial release in the CSSE spectrum and the stepwise heating spectrum (*black pattern*), while the early dissolution of feldspars is represented by the *hatched pattern*

pare their release characteristics by stepwise heating and by stepwise etching. One striking feature of comparing the spectrum of the control sample by stepheating (SH) with that by closed-system etching has been pointed out above: the CSSE spectrum rises monotonically, while the SH spectrum is much more irregular, with a tendency to a hump shape. The trajectories defined by the data points with increasing temperature indicate that sequential breakdown controls the shape of the spectra. Indeed, biotite is degassed early on in SH and is easily leached (Fig. 7e); feldspars are readily leached, but sluggishly decomposed in-vacuo (Fig. 3a), thus K-feldspar + plagioclase mixtures are expected to degas early in the CSSE release but late in SH. Pure hornblende, which accounts for most of the gas in all analyzed aliquots, dominates the gas release in the last etching steps but in mid-temperature steps during stepwise heating.

Finally, some hornblendes display staircase-shaped spectra. While the compelling evidence of Rex et al. (1993) shows the importance of biotite admixtures, and the present work has provided a diagnostic framework to reveal biotite and feldspar impurities (Fig. 3), it may still be that some of the age discordance of staircase-shaped spectra could be observed even in a pure hornblende.

Staircase-shaped spectra have been observed on the MMwr-H aliquots both by SH and by CSSE even for those parts of the spectrum that have a high Ca/K ratio. Such parallelism of SH and CSSE can be explained by model (2) just described. Hornblendes exhibit irregularly distributed small patches of very high dislocation density (see earlier). These are likely to be both easier to etch and more prone to geological Ar* loss (due both to fast diffusion paths and small effective grain sizes in these areas). Differences in thermal decomposition may be the mechanism relating geological loss to the in-vacuo heating. Since lattice breakdown reactions during in-vacuo heating nucleate preferentially on planar defects, as implied by the spatial distribution of incipient melting imaged by Lee et al. (1991, Fig. 5a) and Wartho et al. (1991, Fig. 1b), these patches may be thermally less stable than the patches with low dislocation density and decompose at slightly lower crucible temperatures.

The very existence of staircase spectra is very difficult to explain without assuming sequential breakdown. If staircase spectra were really the one-to-one image of concentric gradients, then they would necessarily be associated with an Arrhenian behaviour because of the assumption that the lattice (albeit not necessarily in its low-temperature form) remains stable during the portion of the release associated with the increasing step ages. However, this has long been shown not to be the case, as the Arrhenius plots of in-vacuo heated samples give apparent diffusivities that are unsuitable to characterize Ar retention in a geological environment (Gaber et al. 1988).

In-vacuo Arrhenius systematics

If Arrhenius diagrams obtained from in-vacuo heating do not provide a measure of Fickian diffusion of Ar out of hornblendes, then the question raised is: what is the rate-controlling process being displayed in such diagrams (e.g. Gaber et al. 1988, Fig. 8)?

During in-vacuo heating, hornblende first undergoes lattice dehydration, followed by several decomposition reactions studied by Lee et al. (1991) and Wartho et al.

(1991). Consequently, an Arrhenius plot of the apparent diffusivity is not expected to be linear as it pertains to more than one process over the whole temperature range, and indeed shows two points of inflection near 880 and 1050 °C, two critical temperatures according to Lee et al. (1991) and Wartho et al. (1991). In this sense, the Arrhenius diagram can be used as a "probe" of the ongoing process: the apparent bulk diffusivity does reflect the progress of the in-vacuo reactions that control Ar release.

Thus, it is meaningful to compare the apparent bulk diffusivity of the untreated aliquot MMwr-C with that of the heated run -H (for convenience we display the higher resolution experiment H2). If the amphibole lattice had been modified by the hydrothermal run, the breakdown characteristics would be modified as well, and this would show up as a different trajectory on an Arrhenius plot. We investigated this question by comparing the behaviour of ^{37}Ar release (the Ca-derived isotope is not affected by the phyllosilicate impurities) and calculated the apparent diffusivities of ^{37}Ar (Fig. 9). MMwr-C and -H have indistinguishable Arrhenius trajectories. It is necessary to reiterate that these trajectories do not allow deconvolution of concentric gradients in a distribution of Fickian "domains" in hornblende, but mirror the rate law of a sum of non-Fickian decomposition reactions. Our stepwise heating data imply that these decomposition reactions took place in the same way at the same temperatures both in MMwr-C and -H; this in turn implies that there was no major structural modification of the hornblende lattice during the 846 °C hydrothermal run, confirming the TEM observations presented already.

The MMwr trajectories in Fig. 9 can be compared with those reported by Harrison (1981). Unheated sample 77–600 agrees with MMwr both in shape and in absolute *T* dependence. This suggests that the in-vacuo decomposition of these two hornblendes was identical. In contrast, the trajectory of heated run R82 has a similar shape but is displaced by ©50 K towards lower temperatures. The reason may be either variable decomposition due to variable amphibole composition, or a real lattice degradation (in which case the Ar loss in run R82 pertains to the latter and not to volume diffusion), or a systematic inaccuracy of crucible thermometry in Harrison's (1981) run R82 (inaccuracies of up to 50 K are possible in resistance ovens according to Foland et al. 1993).

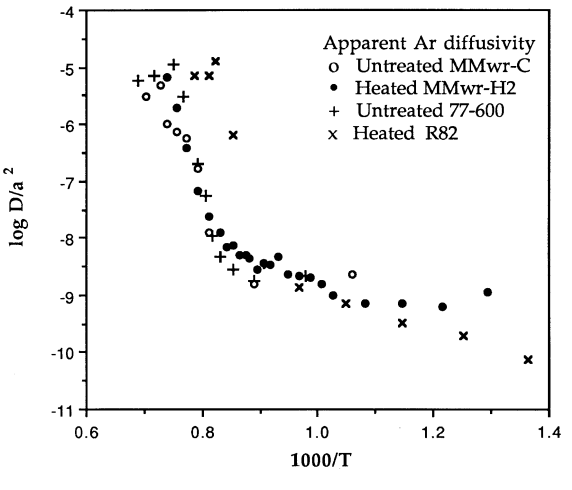

Fig. 9 Arrhenius diagram of in-vacuo release of ^{37}Ar during stepwise heating. *Open symbols*, MMwr-C; *classed symbols*, MMwr-H2; *crosses*, R 82; *plusses*, 77–600. Note that apparent "diffusivity" is not Fickian diffusion but a sum of decomposition reactions; see text for discussion

Discussion of literature data

A further corollary of the present study is that the normally accepted argon diffusion parameters (Harrison 1981) are probably systematically biased, due to the lack of a correction for a phase outgassed at low temperature with a low Ca/K ratio. It is possible to re-examine the original data and attempt their re-evaluation in the light of the insights gained by the present study.

Table 4 of Harrison (1981) shows that for the low-temperature heating steps (T<825 °C) the Ca/K ratio is <4.8 (mineral mixture 1, hereafter subscript 1) while for T>900 °C, Ca/K>12 (mineral mixture 2, hereafter subscript 2). The ratios $(40Ar^*/39Ar)_1$ = 6.62, $(40Ar^*/39Ar)_2$ = 92.65; the value in the untreated sample was 104.1: mineral mixture 1 was 95% degassed, while mixture 2 only suffered 11% loss.

Harrison (1981) assigns errors of 1% on F values. Using his assignments (and correcting run 82 for a typographic error), uncertainties on log D are calculated in order to assess the dispersion of the data points about the fit line (see Villa and Puxeddu 1994, where this was undertaken for biotite). The 8 points of sample 77–600 from Table 3 of Harrison (1981) were regressed using a York routine, and yielded E = 61.1 + 7.8 kcal/mol, log D_0 = −2.19 + 3.77, MSWD = 12. The errors are rather higher than those given by Harrison (1981). The high MSWD clearly shows that use of a single regression line is not justified by the data.

Harrison (1981) used three low-temperature field-based diffusivity estimates to argue that natural and laboratory diffusivities are identical and thus to better constrain the fit through the laboratory data points. However, Wartho (1995, p. 404) has shown that those field estimates are affected by chemical reequilibration and thus cannot be used to deduce a diffusivity for hornblende.

We attempted to correct for the admixture of the low Ca/K contaminant phase. This unrecognized phase is likely to be biotite both because of its frequent petrologic association with magmatic hornblende and because of the difficulty in separating cleanly two minerals having great magnetic and gravimetric similarities. Following this tentative identification, a modal abundance of 5.4% stoichiometric biotite explains the observed spectra of sample 77–600. We used this contamination level throughout; such a high modal abundance of biotite suggests that it was present as fine-grained intergrowths es-

caping visual detection (©10 mm). The latter were most likely completely degassed in all runs, as upheld by $(40Ar*/39Ar)_1 = 6.62$ above. The resulting revised diffusivities have extremely large errors except three: 775 °C, 850 °C (16 m) and 900 °C. Fitting the 6 points between 775 and 900 °C gives E = 64.6 + 26.1 kcal/mole, log $D_0 = -1.68 + 5.03$, MSWD = 2.4. The errors are considerably larger than without the biotite correction; the dispersion is borderline between acceptance and rejection (the calculated probability that the scatter is analytical is 4.8%).

As mentioned already, from the present experiment we can calculate a diffusivity D(846 °C) approximately one order of magnitude lower than that calculated from Harrison's (1981) stated E and D_0, log (D(846 °C)) = −14.13: our two repeat measurements give −15.19 and −14.88. This means that the Ar diffusion in hornblende is *slower* than previously assumed based on Harrison (1981).

Finally, it is noteworthy that field-based estimates of closure temperatures are not an unattractive option, especially when compared with the five orders of magnitude uncertainty of corrected hydrothermal data. The problem with field studies is that it is vital to restrict analysis to samples that: (1) underwent dry metamorphism (so diffusion is not enhanced by alteration due to water influx); (2) were not pervasively deformed (as deformation-induced recrystallization would expel incompatible elements such as accumulated $^{40}Ar*$), and (3) were not retrogressed during exhumation. Possible suitable candidates for a field determination of hornblende closure in a water-poor environment are the synkinematic hornblendes of the 2.00 Ga Limpopo orogeny (Kamber et al. 1995). These authors compared *pT* determinations with Pb/Pb ages on garnets and sphene and proposed that hornblendes, depending on their lattice characteristics, may become closed systems for Ar diffusion as high as 580 °C under cooling rates of 0.7 K/Ma.

Conclusions

By a combination of several different analytical techniques, we have been able to demonstrate:

1. Planar defects with a very narrow spacing exist in the MMwr hornblende. In the untreated hornblende, both halloysite-filled and unfilled cleavages coexist. These planar defects acted as fast diffusion pathways for the diffusion of atmospheric Ar into the hornblende in the hydrothermal experiment (see 3) but it is not clear to what extent they affected the Ar loss.

2. Bulk Ar loss in hydrothermal experiments occurs to a large extent from intergrowths of low-Ca/K minerals such as biotite and degradation products. Genuine volume diffusion from hornblende *sensu stricto* was not detectable in our experiments, but is postulated to exist by analogy with natural metamorphic conditions (Kelley and Turner 1991).

3. The rate constant of bulk Ar loss in hydrothermal laboratory runs is different from, and higher than, that in natural samples. A possible explanation of this observation is that all cleavages were exploited in the experiment, but not all were filled with alteration minerals i.e. had been active as fast Ar loss pathways in the natural environment. This forces a revision of those estimates of Ar retentivity in hornblende that are based on hydrothermal runs, as the latter are not an adequate analogue of natural systems.

4. The discordance observed in hornblende age spectra is largely an artefact of the imperfect mineral separation. The presence of mineral impurities can be revealed by three-isotope correlation diagrams such as Cl/K versus Ca/K. Argon release in successive steps does not mirror concentric concentration gradients but instead results from progressive breakdown reactions of the different minerals in the sample. The absence of a statistically strict plateau in MMhb-1 by stepwise heating and the staircase shape of the CSSE-C spectrum are both effects of the same cause, the presence of ubiquitous submicroscopic impurities in the hornblende.

5. Prudence is required at all times when interpreting $^{39}Ar/^{40}Ar$ dating experiments and inferring thermal histories from them, to avoid stretching results beyond independent geological evidence. Inaccuracies will certainly result if included impurity phases are not recognized; diagnostic tools include comparing the chemical information provided by isotope correlation plots with electron microprobe analyses or petrology. Thermal histories are meaningful only where temperature is the rate-controlling parameter, i.e. for fluid-free, recrystallization-free samples; in those cases, field estimates of thermal closure of hornblende approaching 600 °C corroborate the low "true hydrothermal diffusivity" obtained after artefact corrections in hydrothermal experiments.

Acknowledgements Discussions with H. Baur and P. Signer at a workshop organized by F. Begemann helped inspire this project in 1988. E.C. Alexander Jr, provided the whole rock sample, C. Quercioli assisted with the separation, and D.R. Veblen made available the microscopy equipment. Thanks are due to B.J. Giletti for his encouragement in taking closer looks at "established" literature. Reviews by P.S. Dahl and an anonymous referee are gratefully acknowledged.

References

Alexander EC Jr, Mickelson GM, Lanphere MA (1978) MMhb-1: a new $^{40}Ar/^{39}Ar$ dating standard. US Geol Surv Open File Rep 78–701: 6–8

Baldwin SL, Harrison TM, FitzGerald JD (1990) Diffusion of ^{40}Ar in metamorphic hornblende. Contrib Mineral Petrol 105: 691–703

Berger GW (1975) $^{40}Ar/^{39}Ar$ step heating of thermally overprinted biotite, hornblende and potassium feldspar from Eldora, Colorado. Earth Planet Sci Lett 26: 387–408

Berner RA (1981) Kinetics of weathering and diagenesis. Rev Mineral 8: 111–134

Blanckenburg Fv, Villa IM (1988) Argon retentivity and argon excess in amphiboles from the garbenschists of the Western

Tauern Window, Eastern Alps. Contrib Mineral Petrol 100: 1–11
Dolfi D, Trigila R (1988) Chemical relations between clinopyroxenes and coexisting glasses obtained from melting experiments on alkaline basic lavas. Rend Soc Ital Mineral Petrol 43: 1101–1110
Dunai T, Touret JLR, Villa IM (1992) Mantle derived helium in fluid inclusions of a 2.5 Ga granulite, Nilgiri Hills, Southern India. In: Kaharaka YK, Maest AS (eds) Water-rock interaction, Balkema, Rotterdam, 919–922
Foland KA (1983) $^{40}Ar/^{39}Ar$ incremental heating plateaus for biotites with excess Ar. Chem Geol 41: 3–21
Foland KA, Xu YP (1990) Diffusion of ^{40}Ar and ^{39}Ar in irradiated orthoclase. Geochim Cosmochim Acta 54: 3147–3158
Foland KA, Fleming TH, Heimann A, Elliott DH (1993) Potassium-argon dating of fine-gained basalts with massive Ar loss: application of the $^{40}Ar/^{39}Ar$ technique to plagioclase and glass from the Kirkpatrick Basalt, Antarctica. Chem Geol 107: 173–190
Gaber LJ, Foland KA, Corbató CE (1988) On the significance of argon release from biotite and amphibole during $^{40}Ar/^{39}Ar$ vacuum heating. Geochim Cosmochim Acta 52: 2457–2465
Giese RF (1988) Kaolin minerals: structures and stabilities. Rev Mineral 19: 29–66
Graf T, Signer P, Wieler R, Herpers U, Sarafin R, Vogt S, Fieni C, Pellas P, Bonani G, Suter M, Wölfli W (1990) Cosmogenic nuclides and nuclear tracks in the chondrite Knyahinya. Geochim Cosmochim Acta 54: 2511–2520
Hanson GN, Gast PW (1967) Kinetic studies in contact metamorphic zones. Geochim Cosmochim Acta 31: 1119–1153
Hanson GN, Simmons KR, Bence AE (1975) $^{40}Ar/^{39}Ar$ age spectrum ages for biotite, hornblende and muscovite in a contact metamorphic zone. Geochim Cosmochim Acta 39: 1269–1277
Harrison TM (1981) Diffusion of ^{40}Ar in hornblende. Contrib Mineral Petrol 78: 324–331
Hart SR (1964) The petrology and isotopic-mineral age relations of a contact zone in the Front Range, Colorado. J Geol 72: 493–525
Jäger E, Niggli E, Wenk E (1967) Rb-Sr Altersbestimmungen an Glimmern der Zentralalpen. Beitr Geol Karte Schweiz, NF Liefg 134, Kümmerly and Frey, Bern: 5–67
Kamber BS, Blenkinsop TG, Villa IM, Dahl PS (1995) Proterozoic transpressive deformation in the Northern Marginal Zone, Limpopo Belt, Zimbabwe. J Geol 103: 493–508
Kelley SP (1994) Ar-Ar dating by laser microprobe. In: Potts PJ, Bowles JFJ, Reed SJB, Cave MR (eds) Microprobe techniques in earth sciences. Chapman and Hall, 327–358
Kelley SP, Turner G (1987) Laser probe ^{40}Ar-^{39}Ar age profiles across single hornblende grains from the Giants Range granite, northern Minnesota, USA. Terra Cognita 7: 285
Kelley SP, Turner G (1991) Laser probe ^{40}Ar-^{39}Ar measurements of loss profiles within individual hornblende grains from the Giants Range Granite, northern Minnesota, USA. Earth Planet Sci Lett 107: 634–648
Kelley SP, Trigila R, Villa IM, Wieler R (1991) Assessing the diffusion of Ar in hornblende. Terra Abstr 3: 502
Lee JKW (1993) The argon release mechanisms of hornblende in vacuo. Chem Geol 106: 133–170
Lee JKW, Onstott TC, Cashman KV, Cumbest RJ, Johnson D (1991) Incremental heating of hornblende in vacuo: implications for $^{40}Ar/^{39}Ar$ geochronology and the interpretation of thermal histories. Geology 19: 872–876
Livi KJT, Veblen DR (1987) "Eastonite" from Easton, Pennsylvania: a mixture of phlogopite and a new form of serpentine. Am Mineral 72: 113–125
MacInnis IN, Brantley SL (1993) Development of etch pit size distributions on dissolving minerals. Chem Geol 105: 31–49
Mellini M, Cundari A (1989) On the reported presence of potassium in clinopyroxene from potassium-rich lavas: a transmission electron microscope study. Mineral Mag 53: 311–314
Onstott TC, Miller ML, Ewing RC, Walsh D (1995) Recoil refinements: implications for the $^{40}Ar/^{39}Ar$ dating technique. Geochim Cosmochim Acta 59: 1821–1834
Phillips D (1991) Argon isotope and halogen chemistry of phlogopite from South African kimberlites: a combined step-heating, laser probe, electron microprobe and TEM study. Chem Geol (Isot Geosci) 87: 71–98
Phillips D, Onstott TC (1988) Argon isotpic zonation in mantle phlogopite. Geology 16: 542–546
Rex DC, Guise PG, Wartho JA (1993) Disturbed $^{40}Ar/^{39}Ar$ spectra for hornblende: thermal loss or contamination? Chem Geol 103: 217–281
Samson SD, Alexander EC Jr (1987) Calibration of the interlaboratory ^{40}Ar-^{39}Ar dating standard, MMhb-1. Chem Geol 66: 27–34
Signer P, Baur H, Wieler R (1993) Closed system stepped etching: an alternative to stepped heating. In: Rokop DJ (ed), Proc Alfred O Nier Symp Inorganic Mass Spectrometry, Los Alamos Natl Lab Publ LA-12522-C, Los Alamos, NM, 181–202
Turner G (1968) The distribution of potassium and argon in chondrites. In: Origin and distribution of the elements, Ahrens LH (ed) Pergamon, Oxford, 387–398
Villa IM (1990) Geochronology and excess Ar geochemistry of the Lhotse Nup leucogranite, Nepal Himalaya. J Volc Geoth Res 44: 89–103
Villa IM (1991) Excess Ar geochemistry in potassic volcanites. Schweiz Mineral Petrogr Mitt 71: 211–225
Villa IM (1992) Datability of Quaternary volcanic rocks: an $^{40}Ar/^{39}Ar$ perspective on age conflicts in lavas from the Alban Hills, Italy. Eur J Mineral 4: 369–383
Villa IM (1994) Multipath Ar transport in K-feldspar deduced from isothermal heating experiments. Earth Planet Sci Lett 122: 393–401
Villa IM (1996) Direct determination of ^{39}Ar recoil distance. Geochim Cosmochim Acta 60: (in press)
Villa IM, Puxeddu M (1994) Geochronology of the Larderello geothermal field: new data and the "closure temperature" concept. Contrib Mineral Petrol 115: 415–426
Wartho JA, Dodson MH, Rex DC, Guise PG (1991) Mechanisms of Ar release from Himalayan metamorphic hornblende. Am Mineral 76: 1446–1448
Wartho JA (1995) Apparent argon diffusive loss $^{40}Ar/^{39}Ar$ age spectra in amphiboles. Earth Planet Sci Lett 134: 393–407
Wieler R, Baur H (1994) Krypton and xenon from the solar wind and solar energetic particles in two lunar ilmenites of different antiquity. Meteoritics 29: 570–580
Wieler R, Baur H, Signer P (1986) Noble gases from solar energetic particles revealed by closed system stepwise etching of lunar soil minerals. Geochim Cosmochim Acta 50: 1997–2017
Wieler R, Graf T, Pedroni A, Signer P, Pellas P, Fieni C, Suter M, Vogt S, Clayton RN, Laul JC (1989) Exposure history of the regolithic chondrite Fayetteville: II. Solar-gas-free light inclusions. Geochim Cosmochim Acta 53: 1449–1459
Wieler R, Anders E, Baur H, Lewis RS, Signer P (1991) Noble gases in "phase Q": closed-system etching of an Allende residue. Geochim Cosmochim Acta 55: 1709–1722
Wijbrans JR, McDougall I (1986): $^{40}Ar/^{39}Ar$ dating of white micas from an Alpine high-pressure metamorphic belt on Naxos (Greece): the resetting of the argon isotopic system. Contrib Mineral Petrol 93: 187–194